LA-UR-96- 2986

CONF-9509389--1

Los Alamos National Laboratory is operated by the University of California for the United States Department of Energy under contract W-7405-ENG-36.

TITLE: # An Exploration of Measures for Comparing Measurements with the Results from Meteorological Models for Mexico City

AUTHOR(S): Michael D. Williams
Michael J. Brown

SUBMITTED TO: Tropicana Resort and Casino, Las Vegas, NV, September 11-13, 1995

Los Alamos

Los Alamos National Laboratory
Los Alamos, New Mexico 87545

FORM NO. 836 R4
ST. NO. 2629 5/81

AN EXPLORATION OF MEASURES FOR COMPARING MEASUREMENTS WITH THE RESULTS FROM METEOROLOGICAL MODELS FOR MEXICO CITY

M. D. Williams* and M. J. Brown*

*Los Alamos National Laboratory, Mail Stop F604, Los Alamos, NM 87545,

Abstract--Los Alamos National Laboratory and Instituto Mexicano del Petróleo have completed a joint study of options for improving air quality in Mexico City. We used a three-dimensional, prognostic, higher-order turbulence model for atmospheric circulation (HOTMAC) to treat domains that include an urbanized area. We tested the model against routine measurements and those of a major field program. During the field program, measurements included: (1) lidar measurements of aerosol transport and dispersion, (2) aircraft measurements of winds, turbulence, and chemical species aloft, (3) aircraft measurements of skin temperatures, and (4) Tethersonde measurements of winds and ozone. We made both graphical and statistical comparisons and we have reported some of the comparisons to provide insight into the meaning of statistical parameters including the index of agreement.

Key word index: Prognostic models, complex terrain, urban air quality, measurement-model comparison, Mexico City

1. INTRODUCTION

The task of developing a comprehensive air quality modeling system for any major city is a difficult one. In order to develop a good understanding of urban air quality in major cities, three major components are needed: (1) measurements, (2) emission inventories, and (3) air quality models. Despite many years of development, none of the components can be considered perfect. Measurements may be accurate, but they may not be representative of what we should know for understanding the air quality situation and for modeling air quality changes (e.g, Thomson, 1986). Emission inventories represent areas of major uncertainties (e.g., Gertler and Pierson, 1991 and Oliver, *et al*, 1993). In cities where there has been considerable work over many years, it appears that the

emissions inventories are inconsistent with ambient measurements. Air quality models have had both successes and failures (e.g., Wilson, 1993).

In this paper, we address measures for comparing meteorological and air dispersion modeling results to measurements in areas of complex terrain where the representativeness of measurements is likely to be spatially limited. We have used the sophisticated HOTMAC model (Higher-Order Turbulence Closure Model for Atmospheric Circulation) to overcome the complexity of the terrain and the relative paucity of meteorological data. We have made direct comparisons between modeled and measured meteorological variables and we have also calculated a variety of statistical parameters for evaluating the comparisons. The comparisons are made in the context of Mexico City.

2. THE METEOROLOGICAL MODELING SYSTEM

The objective of the meteorological modeling was to provide atmospheric transport variables for the dispersion and air chemistry models, and to help provide an understanding of the air quality situation. For major urban areas there are two approaches to defining transport variables. One involves interpolating between measurements to provide winds at all points of interest. The other approach involves modeling winds with a meteorological model that can compute a full, three-dimensional time-dependent wind field. The intent of the latter approach, which we used, is to represent the important physics in detail rather than relying on a dense system of measurements to provide the physics from the measurements alone.

2.1. *Model Formulation*

HOTMAC is a three-dimensional time-dependent model (Yamada and Bunker, 1988). It uses the hydrostatic approximation and a terrain-following coordinate system. HOTMAC solves conservation equations for the horizontal wind components, potential temperature, moisture, turbulent kinetic energy, and the turbulence length scale. HOTMAC describes advection, Coriolis effects, and turbulent transfer of heat, momentum, and moisture. It also describes solar and terrestrial radiation effects, turbulent history effects, and the drag and radiation effects of forest canopies. The lower boundary conditions are defined by a surface energy balance and similarity theory. The local soil heat flux is obtained by solving a soil heat conduction equation that ignores horizontal heat transfer. In an urban context the surface energy balance requires an additional term that

represents the heat released by man's activities. The additional heat, along with differences in thermal and albedo properties between urban and non-urban surfaces, produces the urban heat island.

We used a nested grid system to model the valley of Mexico and its surrounding terrain. The outermost grid has a 18 km spacing and covers the major terrain influences as shown in Fig. 1. The innermost grid which has a 21 by 27 array of cells is depicted as a box within the two outer grids and it embraces the city and its immediately adjacent slopes. The inner grid has a resolution of 2 km. The individual characters plotted on the figure are monitoring sites operated by SEDESOL (Secretaria de Desarollo Social or Secretariat for Social Development). The area in yellow represents the urban area as defined by estimated CO emissions.

3. METEOROLOGICAL MODEL-MEASUREMENT COMPARISONS

Measurements are very important to provide model inputs and to help understand the limitations and performance of the models. For the meteorological model there were six types of measurements that were available to provide insight into the model's performance: (1) surface station winds, (2) rawinsonde profiles, (3) Tethersonde profiles, (4) aircraft meteorological profiles, (5) aircraft elevated winds, and (6) lidar-derived mixing heights. It is important to realize that the model and the measurements do not necessarily represent the same parameter. For example, the surface winds are measured at a single site at a height of 10 meters (which may be measured from the top of a building) and represent one hour scalar averages of the wind direction and wind speed. On the other hand, the model provides one hour ensemble mean vector averages of the wind over a 2 kilometer by 2 kilometer grid with a vertical depth appropriate to the grid cell. The model takes the ground level as the street level and includes the buildings as the above-ground canopy. The measurement sites are usually chosen to be in more open areas, but they may be influenced by nearby buildings or trees.

In this paper we focused on wind direction comparisons for February 21-22, 1991 and mixing height comparisons for February 26, 1991. February is normally a month in which very high levels of ozone are found in Mexico City. In February of 1991 an experimental program was carried out to help understand the conditions that lead to high ozone levels in Mexico City. In our model comparisons we discovered deficiencies in the treatment of the thermal radiation from the atmosphere. We found the problem and

improved the model. Consequently, we have two sets of model results, referred to as old model and new model comparisons to describe.

The simulations were begun with information from the late afternoon and early evening rawinsonde measurements at the airport. The balloons are designed to rise at a rate of about 200 meters per minute. In the Mexico City work, the data were available at increments of about 75 meters in height. About 7 rawinsonde flights were made each day. The upper-level winds used as model input at 2000 and 3000 meters above the surface were based on the rawinsonde measurements.

The low-level winds were obtained from a Tethersonde in the northcentral part of the city by averaging the winds between the surface and 500 meters above the surface. The Tethersonde spends a short time at each height and it takes most of an hour to cover the atmosphere up to the maximum height. In contrast, the rawinsonde takes a much shorter time to traverse the same height and produces data at much larger intervals in height. The model requires an ensemble mean wind and thus the Tethersonde provides a better approximation of the required input.

3.1. *Comparison to surface station winds*

Before we begin model-data comparisons, a word of warning must be given. The model produces volume-averaged, ensemble-mean vector winds. These winds are taken from the grid cells nearest to the monitoring locations. The measurements, which were provided by SEDESOL, represent local, scalar-averaged wind speeds and directions. We use the term scalar-averaging to describe the averaging of the wind directions independent of wind speeds and the averaging of speeds independent of directions. In the scalar averaging of the directions the representation of the current wind direction depends upon the value of the previous wind direction and the range of wind directions is taken as 0. to 540 degrees to prevent misleading averages. For example, if the wind were from 350 degrees one minute and 5 degrees the next, 365 degrees would be used instead of 5 degrees for averaging purposes. In this example, if the range were limited to 360 degrees, a 5 degree wind would have been averaged with a 350 degree wind to provide an average of 172 degrees. In addition to the averaging techniques, stations may have local influences which could not be resolved by the model.

There are two kinds of displays which were developed to help understand the model performance: (1) hourly surface plots in which the model wind vectors are shown along with the measured winds and station locations, and (2) daily time-profile plots in which either the wind direction or the wind speed is compared to the measurements.

In both cases the terrain is also shown as well as the locations of the measurement sites. Figures 2 through 5 show hourly simulations with the new model of the vector fields on the inner grid for the morning, late-morning, afternoon, and near midnight, respectively, for February 21. The dark green in the lower left hand corner of the figures represents the mountains to the southwest of the city. The symbol Y represents the Hangares station of the SEDESOL network, which is located at the airport. The blue arrows show the modeled wind speed and direction (not shown if the winds exceed 5. m/s), while the red arrows show the measured wind speed and direction (no arrow is shown if the data are missing or the speed is zero). The modeled values are at a height of 16 meters in the terrain following coordinate system which corresponds to about 25 meters above the ground. This height was chosen because it is the last height below the highest point of the canopy for which calculations were made.

The 6 am slope winds are well represented as evidenced by stations U and T which are closest to the mountains (Fig. 2). Station B is not well represented, but it generally seems to show anomalous behavior (see Figs. 2-5). The measured winds at city stations such as X and Y show a somewhat different behavior than the modeled winds which might be produced by local effects of buildings. The measurements also suggest that there is more wind convergence over the city than the model shows, as seen by predominately westerly winds on the west side of the city and the predominately easterly winds on the east side of the city. The transition to upslope flows occurred at about 10 am when the model showed a less developed transition than the measurements (Fig. 3). At 1 pm, Fig. 4 shows the afternoon flows with fully developed slope winds. At 11 pm, the drainage winds have reestablished themselves and there is good agreement between the model and the measurements (Fig. 5). These four figures demonstrate the variety of wind conditions which can occur in the valley during a single day. They also show that the model does a reasonably good job of representing the major features.

Time profiles of wind directions at all sites on February 21 and February 22 are shown in Figs. 6 and 7, respectively. In Fig. 6, the two inner grids are shown and the two white points on the lower right hand side are the two 5300 meter plus volcanoes, the central green splotch is Pico de Tres Padres, while the red Y is the airport. The model shows good behavior although there are some large fluctuations in the measurements which may be the result of afternoon clouds.

On February 22 the directions shown in Fig. 7 represent a good agreement near the mountain slopes but the agreement is not as good in the more urban areas. Figures 8 and 9 report similar comparisons between the old model results and the measurements on February 21 and 22, respectively.

3.2. *Rawinsonde Profiles*

A major concern about the measurement of upper-level winds by means of a rawinsonde is the relatively short time over which the rawinsonde measurements are made. The meteorological and air quality modeling comunities are using the rawinsonde winds to provide input to models. The difficulty of a brief measurement period is that it may not be very representative of the average conditions needed by the models. This concern is particularly important during the daytime, when the wind fluctuations are large. One way to investigate this problem is to use the models to estimate what variations could be expected among short-term measurements. Since the effective averaging time of the rawinsonde measurements is very much smaller than the timescale of the convective eddies, one can approximate the variance in the measured mean by using the model-computed velocity fluctuations σ_u and σ_v. Figure 10 is an example of such a comparison for 11 am on February 26, 1991. The solid line shows the measured wind directions by the rawinsonde, the dotted line shows the model predictions, while the asterisks show twenty randomly selected model realizations with the same mean winds. In the lower 50 meters above ground level (agl) only one model height was shown to improve readability. Very close to the surface, the asterisks indicate that most of the winds are consistent with the model, because the turbulent fluctuations are so large. Near the surface there is a high speed tail in the measurements which is likely to be a very local effect or perhaps the balloon has been launched from a point other than the assumed point. The odd feature of a high speed tail is a frequent feature in the rawinsonde measurements. The collapse of the range of the asterisks depicts the lower turbulence levels above the mixing height. Figure 11 reports a similar comparison for 2 pm on February 26, 1991. The wind speeds are slightly higher which reduces the spread in wind directions at the lower heights, however the mixing height has increased to about 2500 meters so that there is more spread aloft.

The large spread in wind directions as shown by the asterisks indicates that the rawinsondes cannot be expected to give us precise wind directions during light wind conditions within the mixed layer. Rawinsondes provide the upper-level winds used to drive the air quality and meteorological models throughout the world.

3.5. *Lidar Mixing Heights*

The lidar mixing heights were determined as the height at which 50% of the horizontal area has a signal characteristic of the clean air aloft. Typically, the lidar cannot

identify structures below about 100 meters because of line of sight restrictions caused by nearby objects.

Figure 12 displays the comparison of mixing heights between the new model and the measurements for February 26, while Figure 13 reports a similar comparison for the old model. The principal disagreements are in the night when the LIDAR minimum heights may be important and in the late afternoon when left-over aerosols cast doubt on the validity of the LIDAR measurements of current mixing. The new model does a much better job of describing the morning increase in the mixing heights that is very important in air chemistry modeling. The older model does a better job of describing the evening collapse of the mixing heights and the afternoon stabilized height. The afternoon heights are somewhat uncertain because the model resolution is rather poor, about 500 meters at heights of 2.5 kilometers. Furthermore, the LIDAR defines the height by the presence of aerosol layers so it may not provide an accurate representation of the evening collapse of the mixing heights because it will sense aerosols left over from an earlier time rather than aerosols freshly mixed aloft from surface sources.

4. METEOROLOGICAL MODEL PERFORMANCE SUMMARY

Tesche et al. (1990) among others, have suggested a suite of statistical and graphical measures for evaluating the performance of photochemical models. Included among the statistical measures are: model means, observational means, standard deviation of model estimates, standard deviation of observations, least-squares regression statistics, root-mean-square error, systematic root-mean-square error, unsystematic root-mean-square error, index of agreement, skill error, and skill variance. The index of agreement is formed by subtracting from 1 the product of number of samples and the squared error divided by the sum over all samples of the squared absolute value of the sample deviation from the sample mean plus the predicted deviation from the sample mean. When the index of agreement is one, the predictions are perfect, while an index of zero means the predictions are noise. The skill error is the ratio of the unsystematic root mean square error to the standard deviation of the observations. The skill variance is the ratio of the standard deviation of the predictions to the standard deviation of the observations.

The computation of these statistical parameters is straight forward for the mixing-layer heights, but wind directions pose a more difficult problem. Because of the difficulty with circular data, techniques developed by Mardia (1972) were used to calculate a regression relationship which is analogous to the standard regression on a line.

Table I summarizes the statistics for wind directions at the monitoring stations for two days with both the old model and the revised model. The sample is composed of 414 hourly averaged values.

Table I. Statistical comparison of model and measurement surface winds and mixing heights.

Parameter	Old Wind Direction	New Wind Direction
Model mean	8.	278.
Observation mean	130	130.
Standard deviation of predictions	103	69.
Standard deviation of observations	98.	98.
Regression intercept	10.	207.
Regression coefficient	1.06	2.48
Correlation coefficient	xx	xx
Root-mean-square error	95.	86.
Systematic root-mean-square error	13.	85.
Unsystematic root-mean-square error	95.	112.
Index of agreement	0.74	0.84
Skill error	1.11	1.14
Skill variance	1.06	0.70

The correlation coefficient for wind directions is not shown, since it is not calculated for circular data. Another way to make the comparison is to make comparisons for the wind

Another way to look at the comparison is by wind components. Unfortunately, wind components introduce an another element, wind speed, that tends to make the apples an oranges character of the comparisons (grid-averaged versus point) even worse. The model treats the domain as an urban canopy whereas the actual measurements are sometimes taken from towers placed on the top of buildings and sometimes made between buildings. There is normally a large increase in wind speed as one moves from a point within the canopy to one somewhat above the canopy. Wind directions have less systematic changes although direction fluctuations associated with building orientations are important. One way to achieve some of the benefits of component comparisons that permit the use of simple scatter plots and regression statistics is to compare the cosine and sine of the measured and modeled, wind directions. Figure 14 shows a comparison between the cosine of the new-model wind directions and the measured wind directions.

Figure 15 shows the comparison between the sine of the measured and modeled wind directions. Figure 16 shows a comparison between the old-model cosine of wind direction and the measured, cosine of wind direction, while Figure 17 shows a comparison between measured and modeled sines of the wind directions. Table III reports the statistical parameters for the new and old model cosine of the wind direction.

Table II Statistical comparison of modeled and measured cosine of wind directions.

Parameter	Old Cosine of Wind Direction	New Cosine of Wind Direction
Model mean	.01	.07
Observation mean	-.06	-.06
Standard deviation of predictions	.68.	.68
Standard deviation of observations	.68	.68.
Regression intercept	.03	.09.
Regression coefficient	.31	.39
Correlation coefficient	.31	.39
Root-mean-square error	.80	.76
Systematic root-mean-square error	.47	.44
Unsystematic root-mean-square error	.65	.62
Index of agreement	.62	.66
Skill error	.95	.91
Skill variance	1.00	.99

Table III reports the statistical parameters for the new and old model sine of the wind direction comparions.Table II Statistical comparison of modeled and measured cosine of wind directions.

Parameter	Old Sine of Wind Direction	New Sine of Wind Direction
Model mean	.00	-.46
Observation mean	.07	.07
Standard deviation of predictions	.73	.57
Standard deviation of observations	.73	.73
Regression intercept	.00	-.48
Regression coefficient	.03	.27

Correlation coefficient	.03	.35
Root-mean-square error	1.02	.92
Systematic root-mean-square error	.71	.75
Unsystematic root-mean-square error	.73	.53
Index of agreement	.48	.60
Skill error	1.00	.73
Skill variance	1.01	.78

While the scatter plots do little to inspire confidence in the model, the winds respond well to major changes in forcing winds and the slope winds develop appropriately and couple well with the large-scale conditions. The statistical parameters, notably the index of agreement suggest that the new model slightly outperforms the old model. Furthermore, the wind direction statistics look beter than the statistics for the individual components. There are some areas, however, which could be improved.

A second illustration of the use of the statistical indices is based on the comparison of modeled mixing layer heights with measurements for both the new and the old model. In this case the sample size is only 14 and the measurements represent averages over several minutes. Figure 18 shows a comparison between the new model mixing heights and the measured mixing heights. Figure 19 is a scatter plot of the old-model mixing heights and the measurements.

Table IV Statistical comparison of model and measurement mixing heights.

Parameter	**Old Mixing Height**	**New Mixing Height**
Model mean	1796.	1179.
Observation mean	1681.	1681.
Standard deviation of predictions	1161.	1053.
Standard deviation of observations	1201.	1201.
Regression intercept	412	37.
Regression coefficient	.82	.69
Correlation coefficient	.85	.77
Root-mean-square error	631.	895.
Systematic root-mean-square error	235.	624.
Unsystematic root-mean-square error	585.	642.

Index of agreement	0.92	0.84
Skill error	.49	.54
Skill variance	.97	0.88

In this instance the statistics parameters would suggest that the old model performs better than the new. However, the graphical representation produces a much different conclusion. The new model underpredicts the height of the mixing height in the afternoon which would tend to produce overestimates of the concentrations by about 20% at a time when the chemistry is relatively stable. The old model however dramatically overpredicts the mixing height in the morning when the concentrations are high and the chemical changes are most rapid. The old model will produce much lower concentrations at a critical time of the day. The principal errors with the new model occur in the model domain where the model results lack precision because of the coarse grid resolution. Furthermore, the differences between the new model and the measurements occur at times when the measurements are may be erroneous, because they don't distinquish between recently transported aerosols and those that were left-over from mixing earlier in the day.

5. SUMMARY AND CONCLUSIONS

We have illustrated the application of the suite of graphical and statistical measures which have been recommended for model evaluation. The application included a case where the performance of an improved model was compared to an earlier version of the model which had an deficient description of some of the physics of the atmosphere. The illustration shows the importance of supplementing statistical measures with graphical displays. The illustration also emphasizes how the interpretation of the statistical measures must be made in the context of an understanding of the deficiencies in the measurements.

We have also presented an example of how the model's description of short-term fluctuations can be used to assess the representativeness of short duration measurements. Rawinsondes are the most widely used technique for measuring upper-level winds for meteorological and air quality modeling. However, our analysis shows that during light-wind, daytime conditions, mean-winds can be expected to be significantly different than those measured by the rawinsonde.

REFERENCES

Gertler, A.W., and W.R. Pierson, (1991) Motor Vehicle Modeling Issues, paper 91-88.8 in Proceedings Volume 7, Air Modeling Papers from the 84th Annual Meeting, published by the Air & Waste Management Association, Pittsburgh, Pennsylvania.

Mardia, K.V.(1972) Statistics of Directional Data, Academic Press Inc., Orlando, Florida, 127-128.

Oliver, W.R., R.J.Dickson, and L. Bruckman (1993) Development of the SCAQS High-Resolution Emissions Inventory: Assessment of Inventory Uncertainties" in Proceedings of an International Specialty Conference, Southern California Air Quality Study, Data Analysis, VIP-26 published by the Air & Waste Management Association, Pittsburgh, Pennsylvania, . 62-73.

Tesche, T.W., P. Georgopoulus, J.H. Seinfeld, G. Cass, F. L. Lurmann, PM Roth (1990) Improvement of Procedures for Evaluating Photochemical Models, final report contract No. A832-103, prepared for the California Air Resources Board, Radian Corporation, DCN:90-264-069-05-02.

Thomson, D. W. (1986) Systems for Measurements at the Surface, in Mesoscale Meteorology and Forecasting, ed. P. Ray, AMS, Boston, 71-84.

Wilson, Robert B., 1993, Review of Development and Application of CRSTER and MPTER Models, *Atmospheric Environment*, . **27B**, pp 41-57.

Yamada, T. and S. Bunker (1988) Development of a Nested Grid, Second Moment Turbulence Closure Model and Application to the 1982 ASCOT Brush Creek Data Simulation *J. Appl. Meteor.*, **27**, 562-578 .

FIGURE CAPTIONS

Figure 1. Model domains for the Mexico City air basin. The blue areas represent the Gulf of Mexico, while the white points are the volcanoes which reach about 4600 m msl.

Figure 2. Comparison of measured winds (red) to computed winds (blue) for 6 a.m., February. 21, 1991, with station locations and topography.

Figure 3. Comparison of measured winds (red) to computed winds (blue) for 11 a.m., February. 21, 1991, with station locations and topography.

Figure 4. Comparison of measured winds (red) to computed winds (blue) for 1 p.m., February. 21, 1991, with station locations and topography.

Figure 5. Comparison of measured winds (red) to computed winds (blue) for 11 p.m., February. 21, 1991, with station locations and topography.

Figure 6. Comparison of measured hourly wind directions (yellow) to computed (new model) hourly wind directions (blue) on February 21,1991, with station locations and topography.

Figure 7. Comparison of measured hourly wind directions (yellow) to computed (new model) hourly wind directions (blue) on February. 22, 1991, with station locations and topography.

Figure 8. Comparison of measured hourly wind directions (yellow) to computed (old model) hourly wind directions (blue) on February. 21,1991, with station locations and topography.

Figure 9. Comparison of measured hourly wind directions (yellow) to computed (old model) hourly wind directions (blue) on February. 22, 1991, with station locations and topography.

Figure 10. Comparison of measured wind directions (green solid) to modeled mean directions (yellow dotted), and to twenty model realizations (asterisks) for 11 am on the 26th of February 1991.

Figure 11. Comparison of measured wind directions (green solid) to modeled mean directions (yellow dotted), and to twenty model realizations (asterisks) for 2 pm on the 26th of February 1991.

Figure 12. Comparison of the LIDAR measured mixing heights (asterisks) to the modeled (new) mixing heights (line) for February 26, 1991.

Figure 13. Comparison of the LIDAR measured mixing heights (asterisks) to the modeled (old) mixing heights (line) for February 26, 1991.

Figure 14. Scatter plot of new model, cosine of wind direction and measurements of the cosine of wind directions at surface stations.

Figure 15. Scatter plot of new model, sine of wind direction and measurements of the sine of wind directions at surface stations.

Figure 16 Scatter plot of old model, cosine of wind direction and measurements of the cosine of wind directions at surface stations.

Figure 17. Scatter plot of old model, sine of wind direction and measurements of the sine of wind directions at surface stations.

Figure 18. Scatter plot of new model, mixing-layer heights and LIDAR measurements mixing-layer height.

Figure 19. Scatter plot of new model, mixing-layer heights and LIDAR measurements mixing-layer height.

Figure 1. Model domains for the Mexico City air basin. The blue areas represent the Gulf of Mexico, while the white points are the volcanoes which reach about 4600 m msl.

Figure 2. Comparison of measured winds (red) to computed winds (blue) for 6 a.m., February. 21, 1991, with station locations and topography.

Figure 3. Comparison of measured winds (red) to computed winds (blue) for 11 a.m., February. 21, 1991, with station locations and topography.

Figure 4. Comparison of measured winds (red) to computed winds (blue) for 1 p.m., February. 21, 1991, with station locations and topography.

Figure 5. Comparison of measured winds (red) to computed winds (blue) for 11 p.m., February. 21, 1991, with station locations and topography.

Figure 6. Comparison of measured hourly wind directions (yellow) to computed (new model) hourly wind directions (blue) on February 21,1991, with station locations and topography.

Figure 7. Comparison of measured hourly wind directions (yellow) to computed (new model) hourly wind directions (blue) on February. 22, 1991, with station locations and topography.

Figure 8. Comparison of measured hourly wind directions (yellow) to computed (old model) hourly wind directions (blue) on February. 21,1991, with station locations and topography.

Figure 9. Comparison of measured hourly wind directions (yellow) to computed (old model) hourly wind directions (blue) on February. 22, 1991, with station locations and topography.

Figure 10. Comparison of measured wind directions (green solid) to modeled mean directions (yellow dotted), and to twenty model realizations (asterisks) for 11 am on the 26th of February 1991.

Figure 11. Comparison of measured wind directions (green solid) to modeled mean directions (yellow dotted), and to twenty model realizations (asterisks) for 2 pm on the 26th of February 1991.

Figure 12. Comparison of the LIDAR measured mixing heights (asterisks) to the modeled (new) mixing heights (line) for February 26, 1991.

Figure 13. Comparison of the LIDAR measured mixing heights (asterisks) to the modeled (old) mixing heights (line) for February 26, 1991.

Figure 14. Scatter plot of new model, cosine of wind direction and measurements of the cosine of wind directions at surface stations.

Figure 15. Scatter plot of new model, sine of wind direction and measurements of the sine of wind directions at surface stations.

Figure 16 Scatter plot of old model, cosine of wind direction and measurements of the cosine of wind directions at surface stations.

Figure 17. Scatter plot of old model, sine of wind direction and measurements of the sine of wind directions at surface stations.

Figure 18. Scatter plot of new model, mixing-layer heights and LIDAR measurements mixing-layer height.

Figure 19. Scatter plot of new model, mixing-layer heights and LIDAR measurements mixing-layer height.

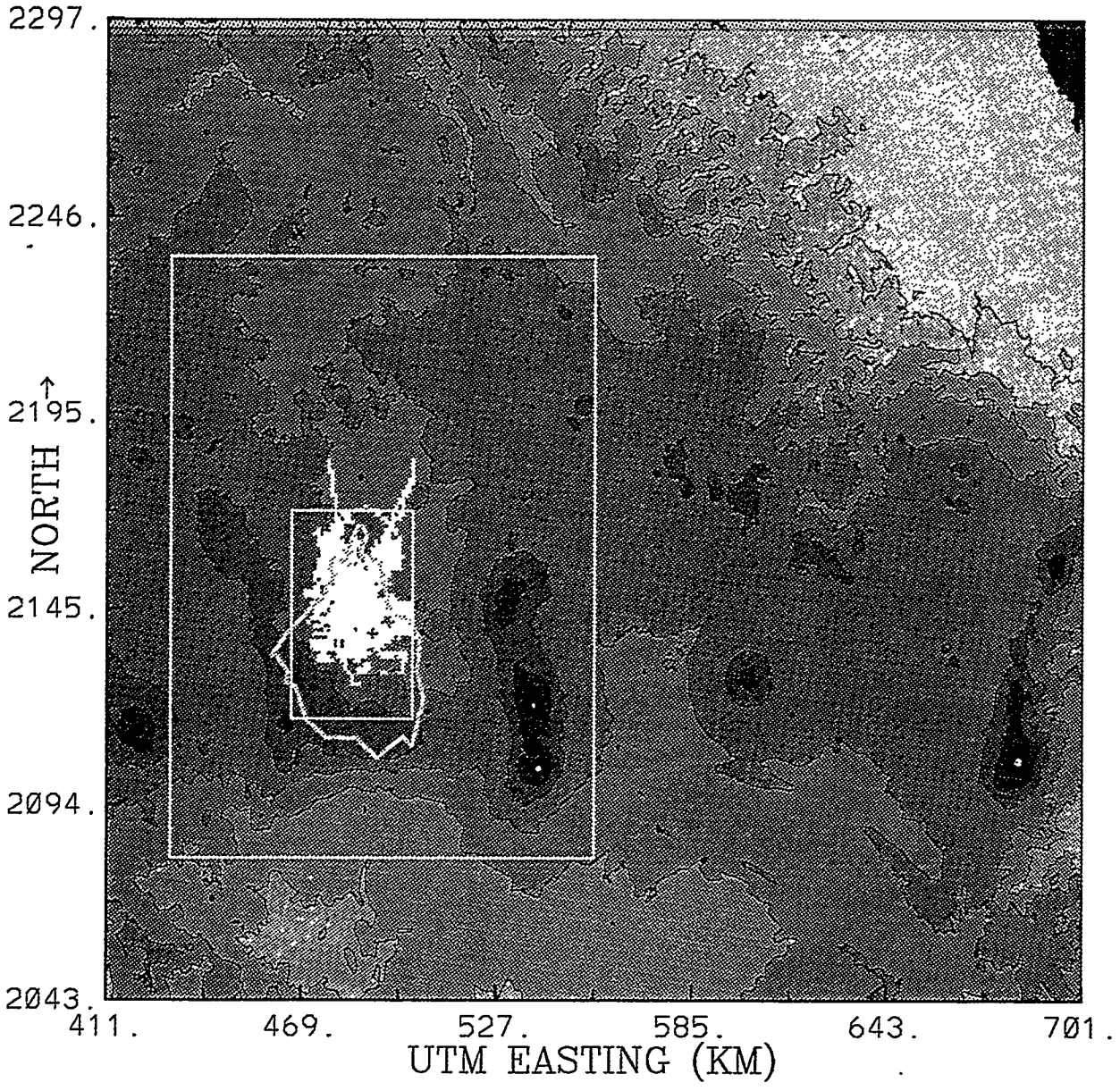
2297.
2246.
2195.
2145.
2094.
2043.
NOR'TH
411.
469.
527.
585.
643.
701.
UTM EASTING (KM)

21 FEB 1991 6 AM

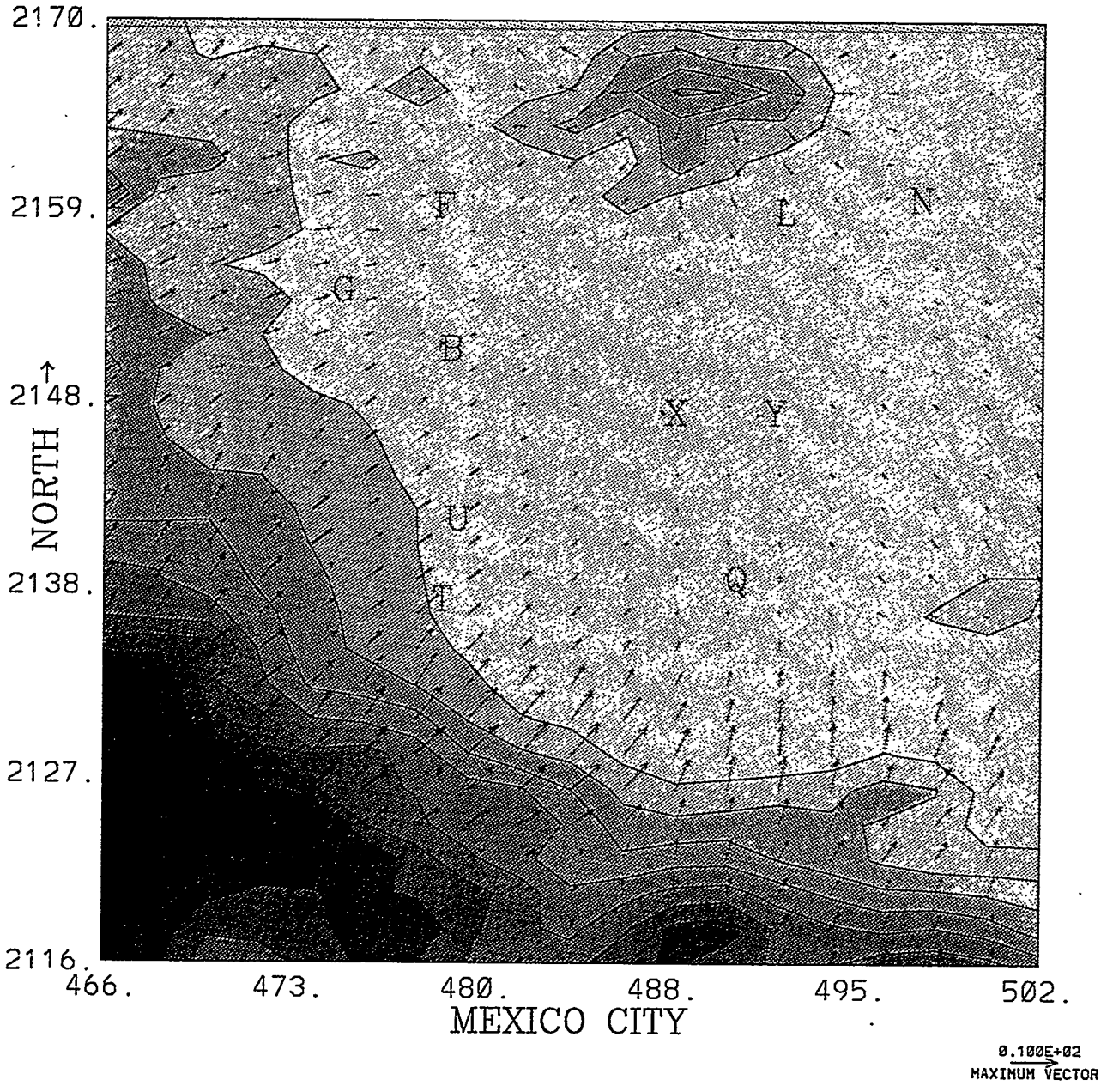

21 FEB 1991 11 AM

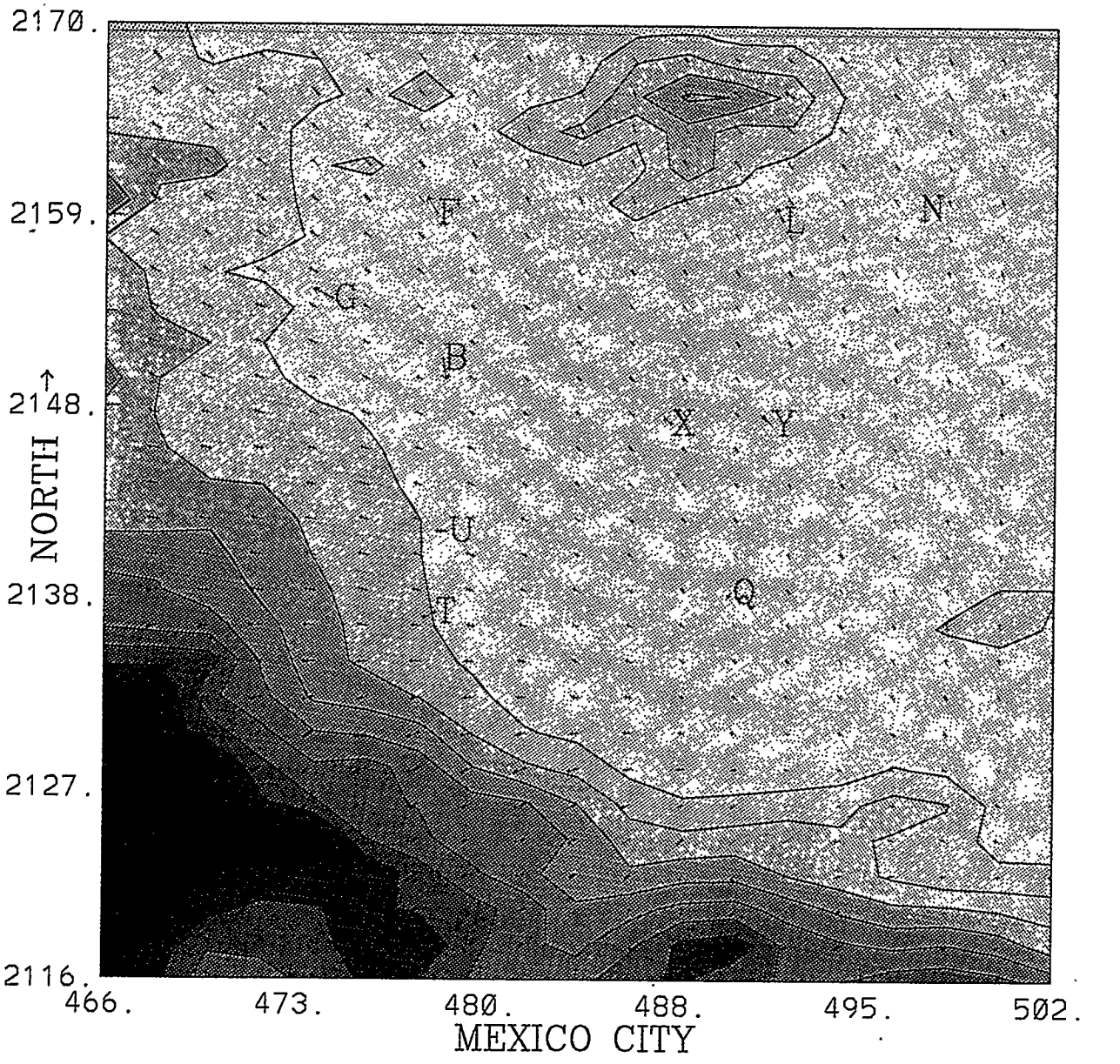

21 FEB 1991 1 PM

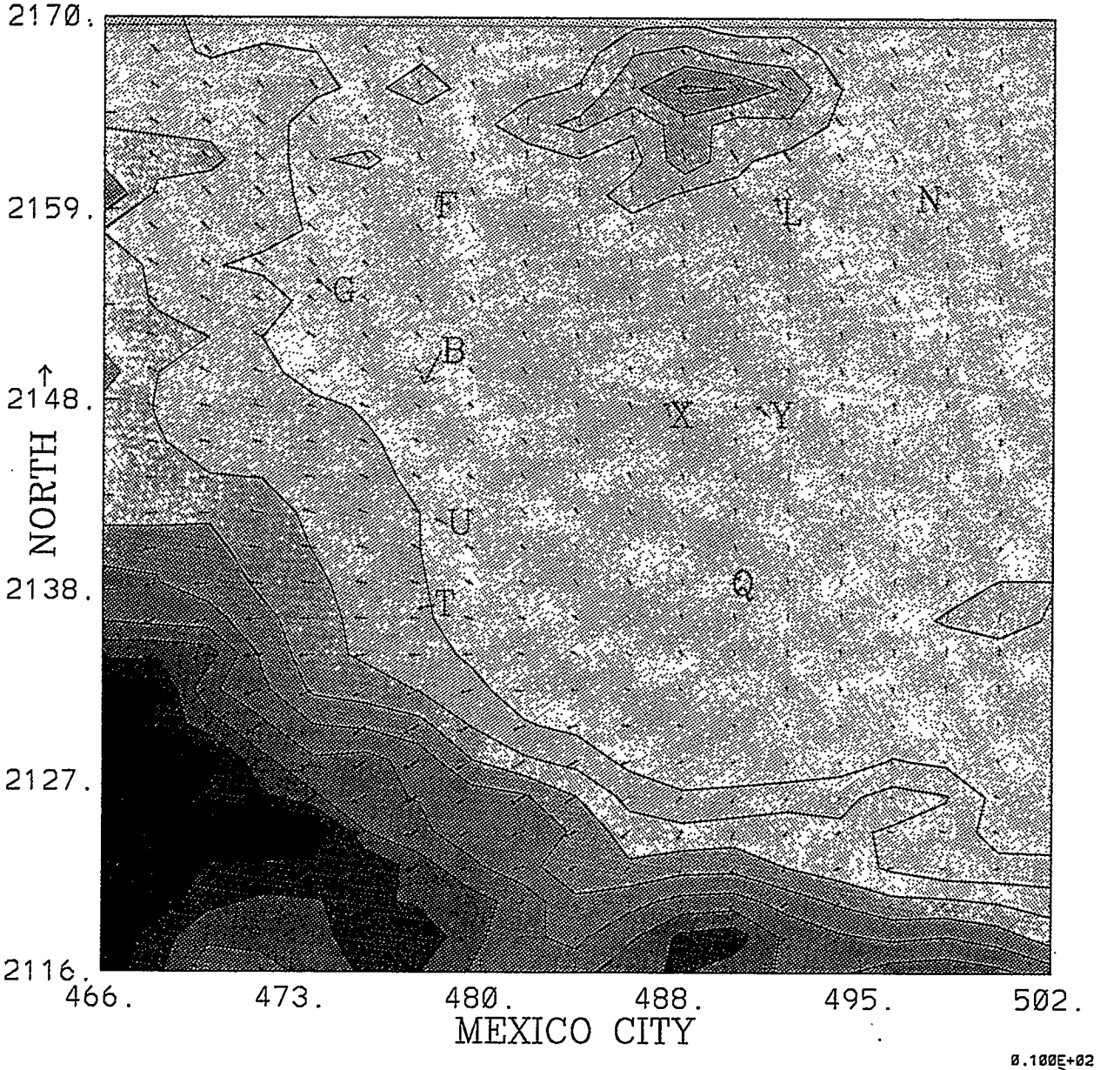

21 FEB 1991 11 PM

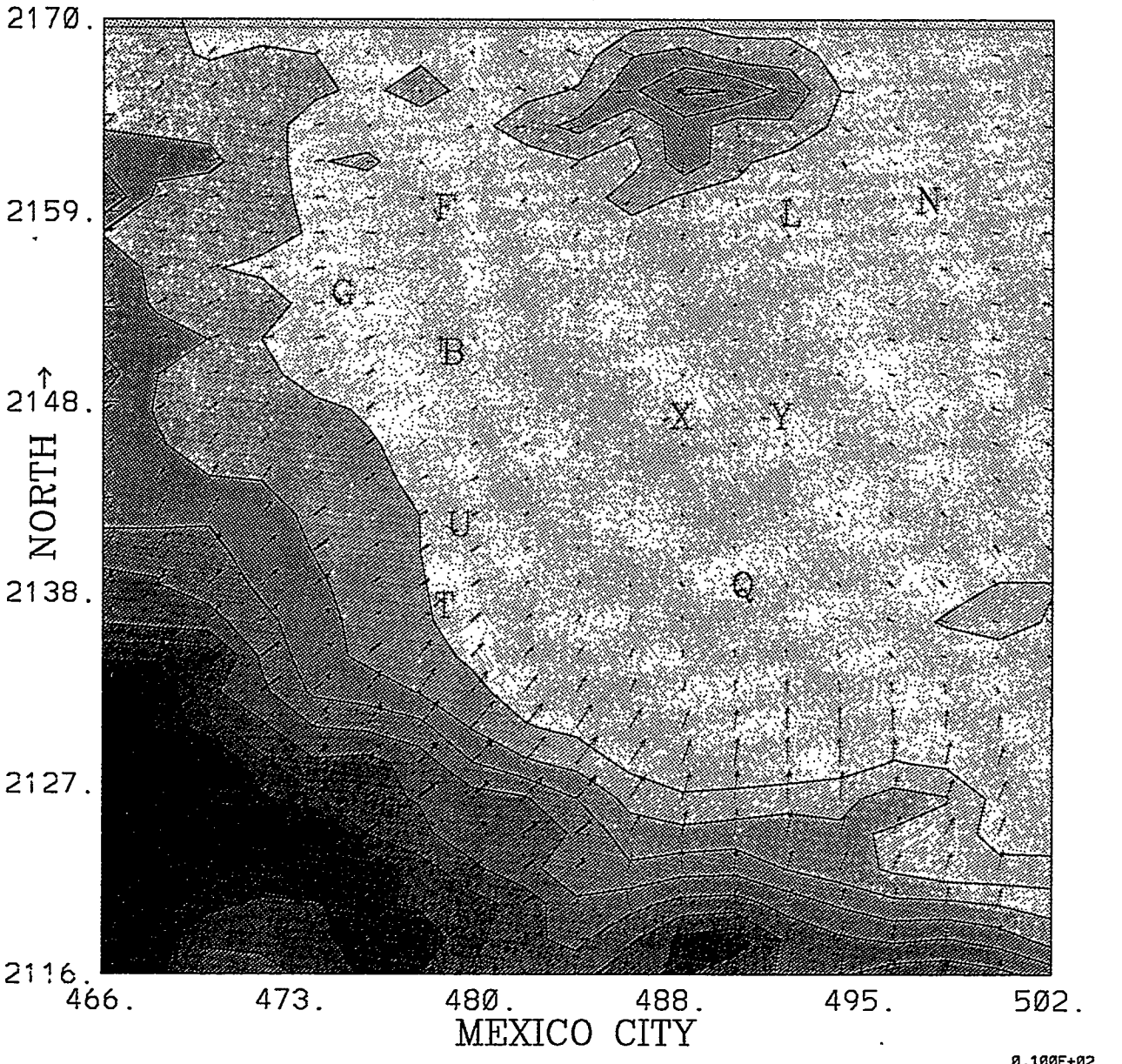

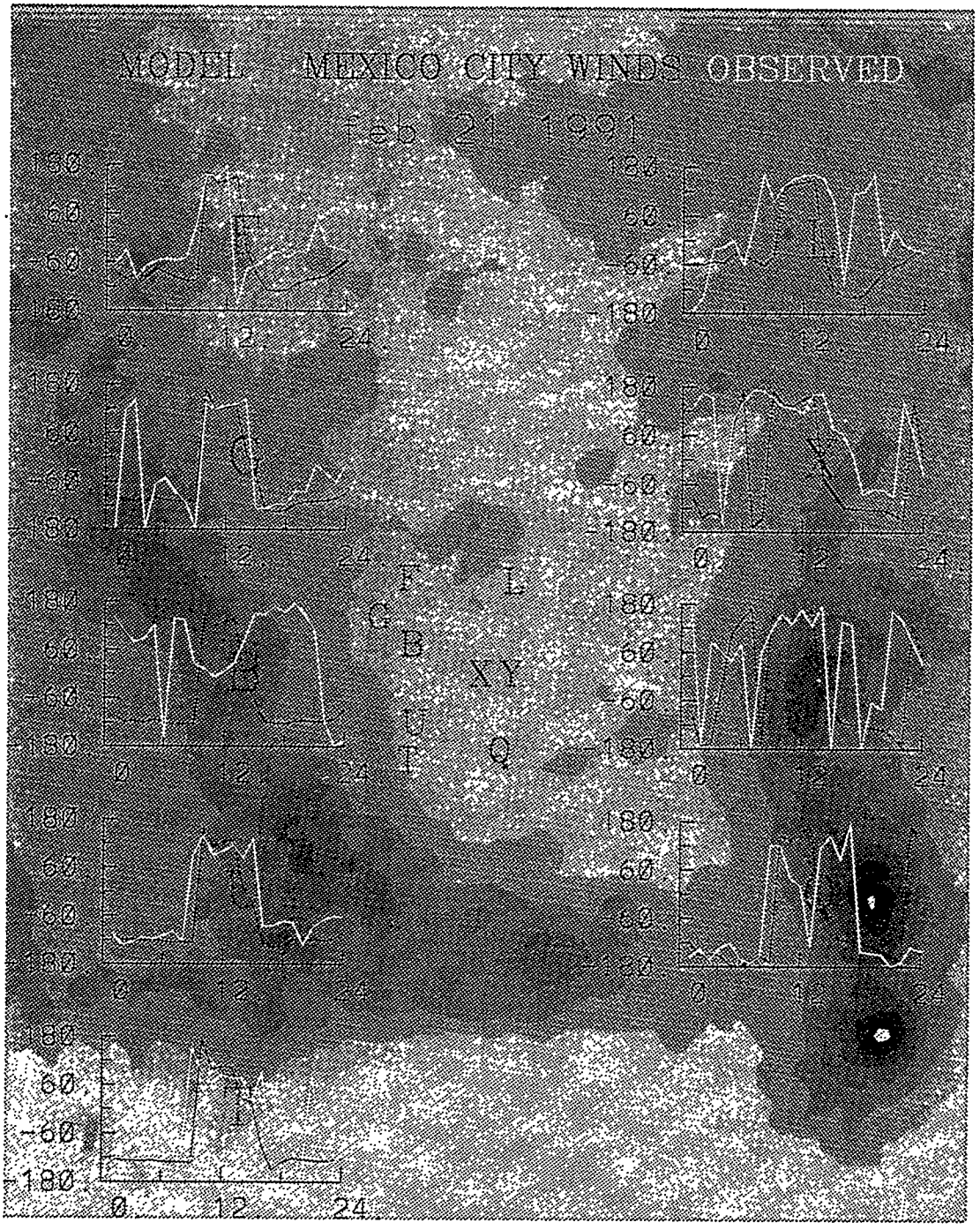
MODEL
MEXICO CITY WINDS
OBSERVED
Feb 21 1991
180
60
-60
-180
0
12
24
F
L
G
D
XY
T
Q

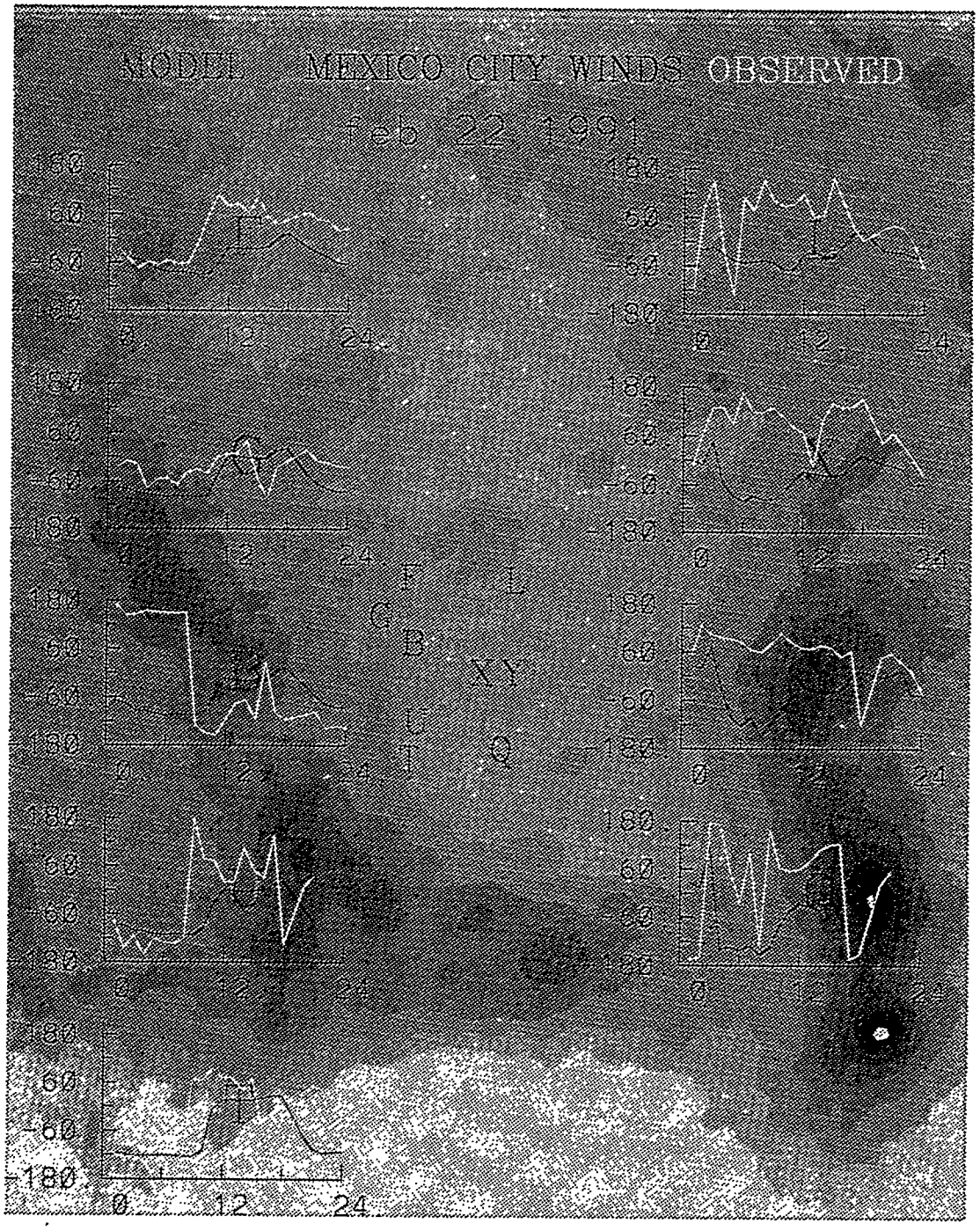
MODEL MEXICO CITY WINDS OBSERVED
feb 22 1991
180
60
-60
-180
0
12
24

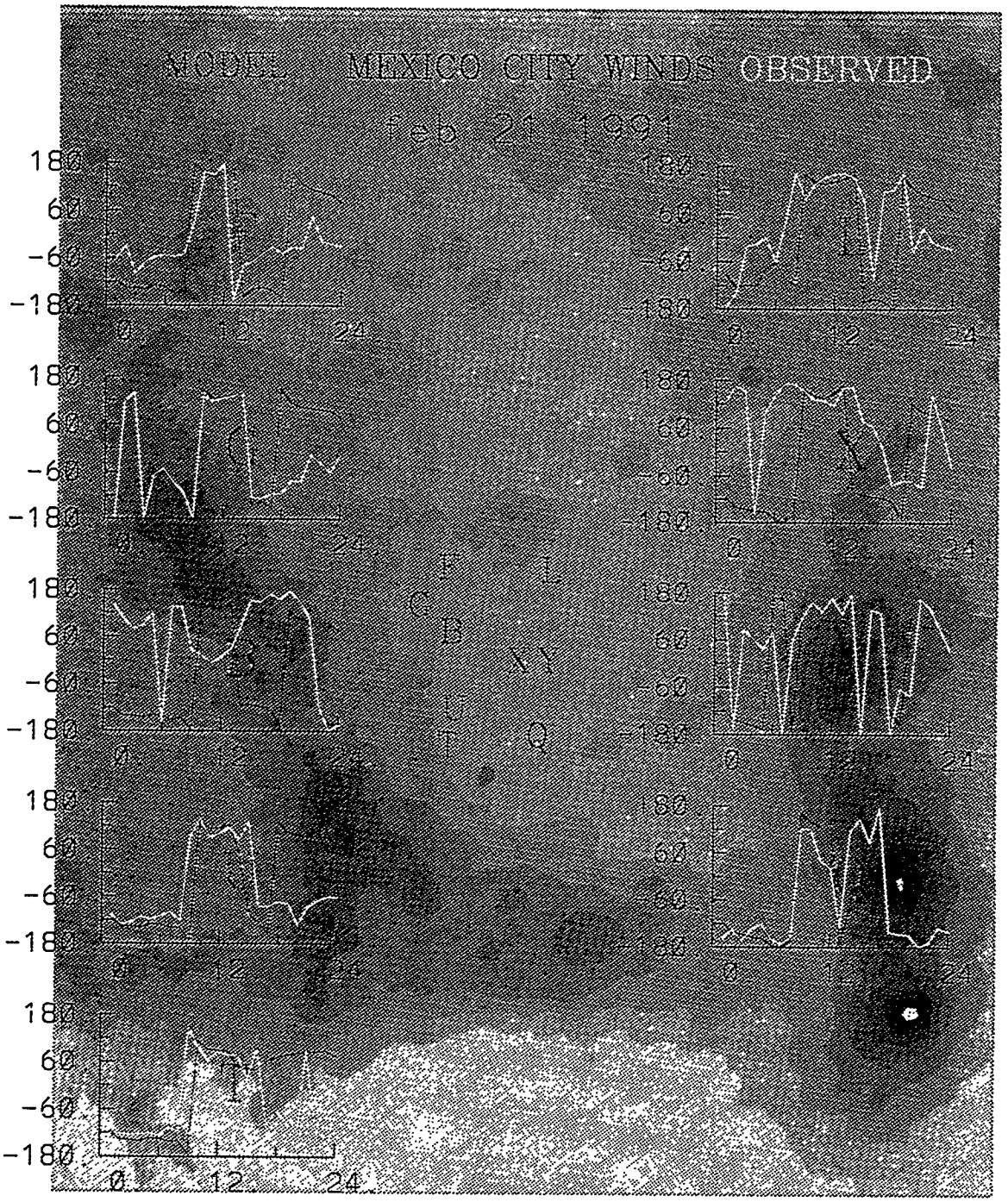
MODEL MEXICO CITY WINDS OBSERVED
feb 21 1991
180
60
-60
-180
0
12
24

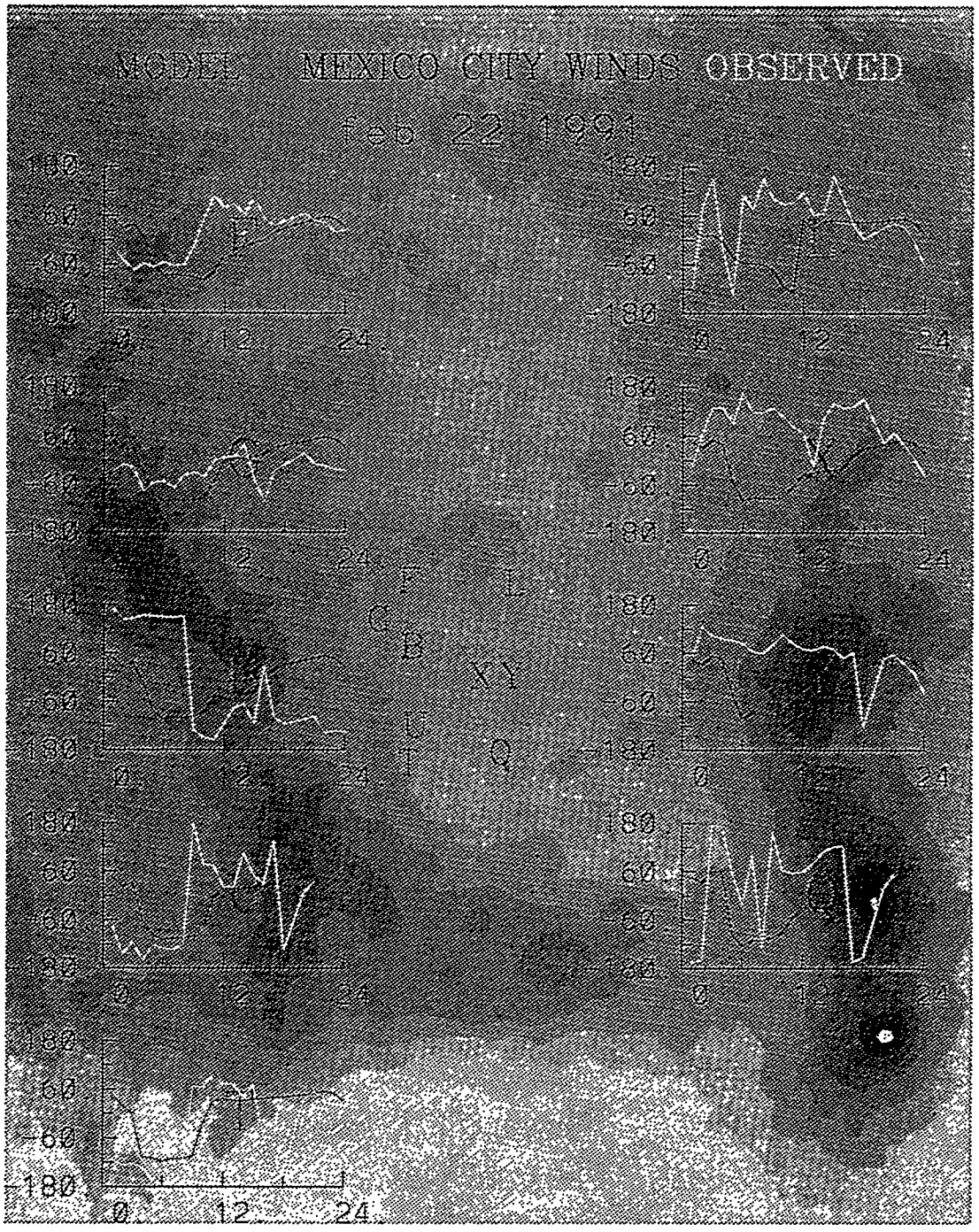
MODEL
MEXICO CITY WINDS OBSERVED
Feb 22 1994
180
60
-60
-180
0
12
24

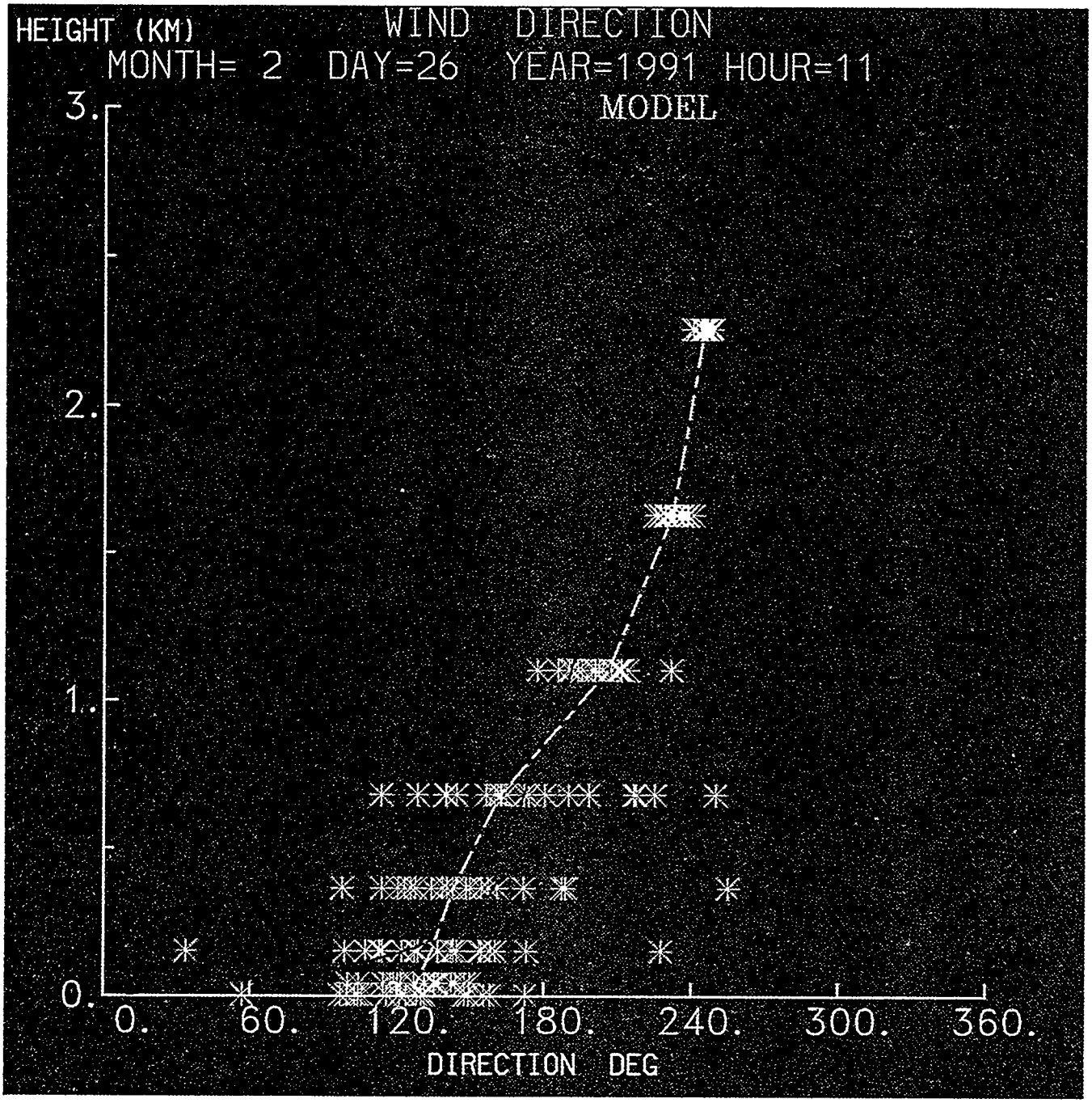
HEIGHT (KM)
WIND DIRECTION
MONTH= 2 DAY=26 YEAR=1991 HOUR=11
MODEL
3.
2.
1.
0.
0.
60.
120.
180.
240.
300.
360.
DIRECTION DEG

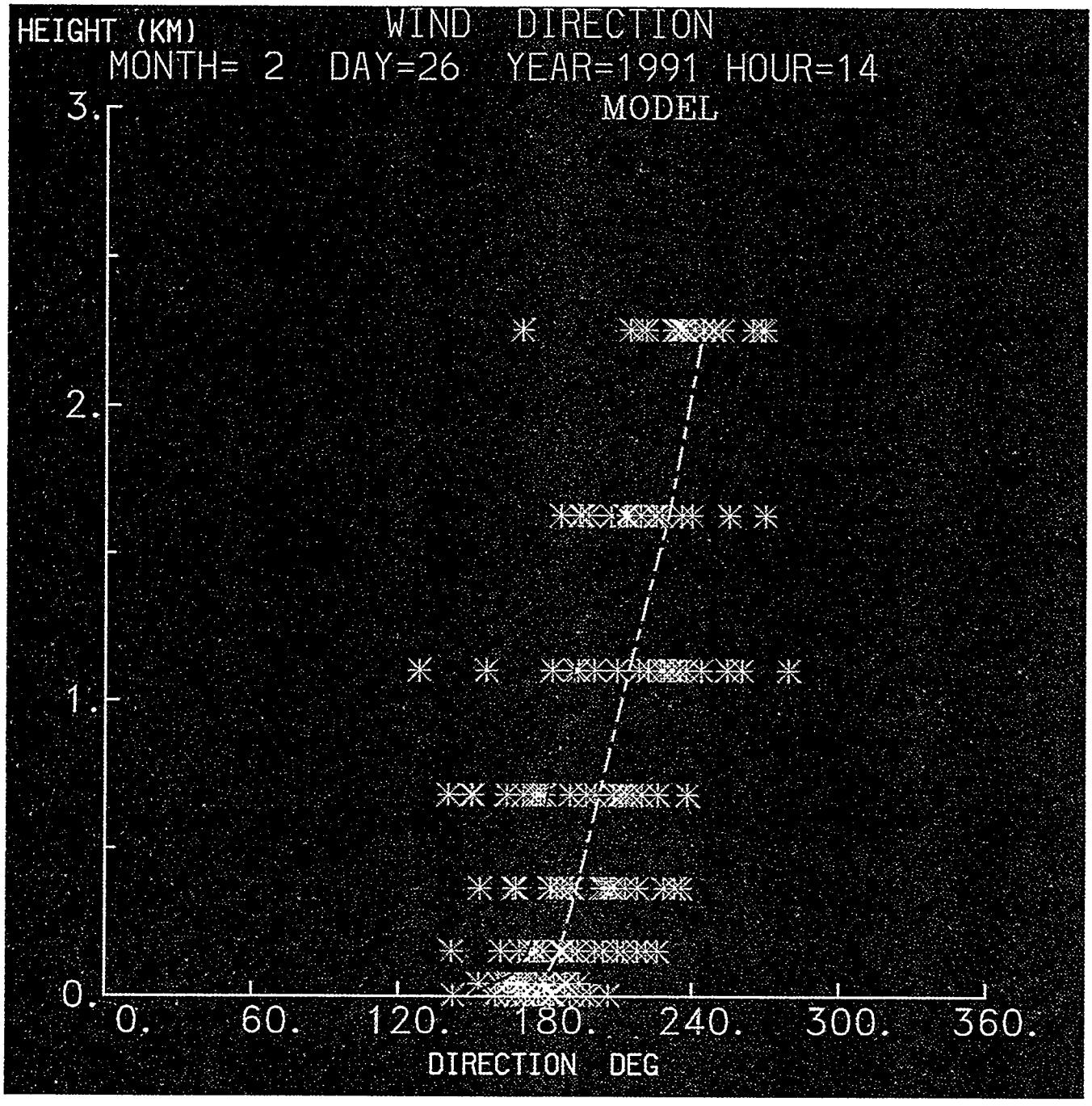
HEIGHT (KM)
WIND DIRECTION
MONTH= 2 DAY=26 YEAR=1991 HOUR=14
MODEL
3.
2.
1.
0.
0.
60.
120.
180.
240.
300.
360.
DIRECTION DEG

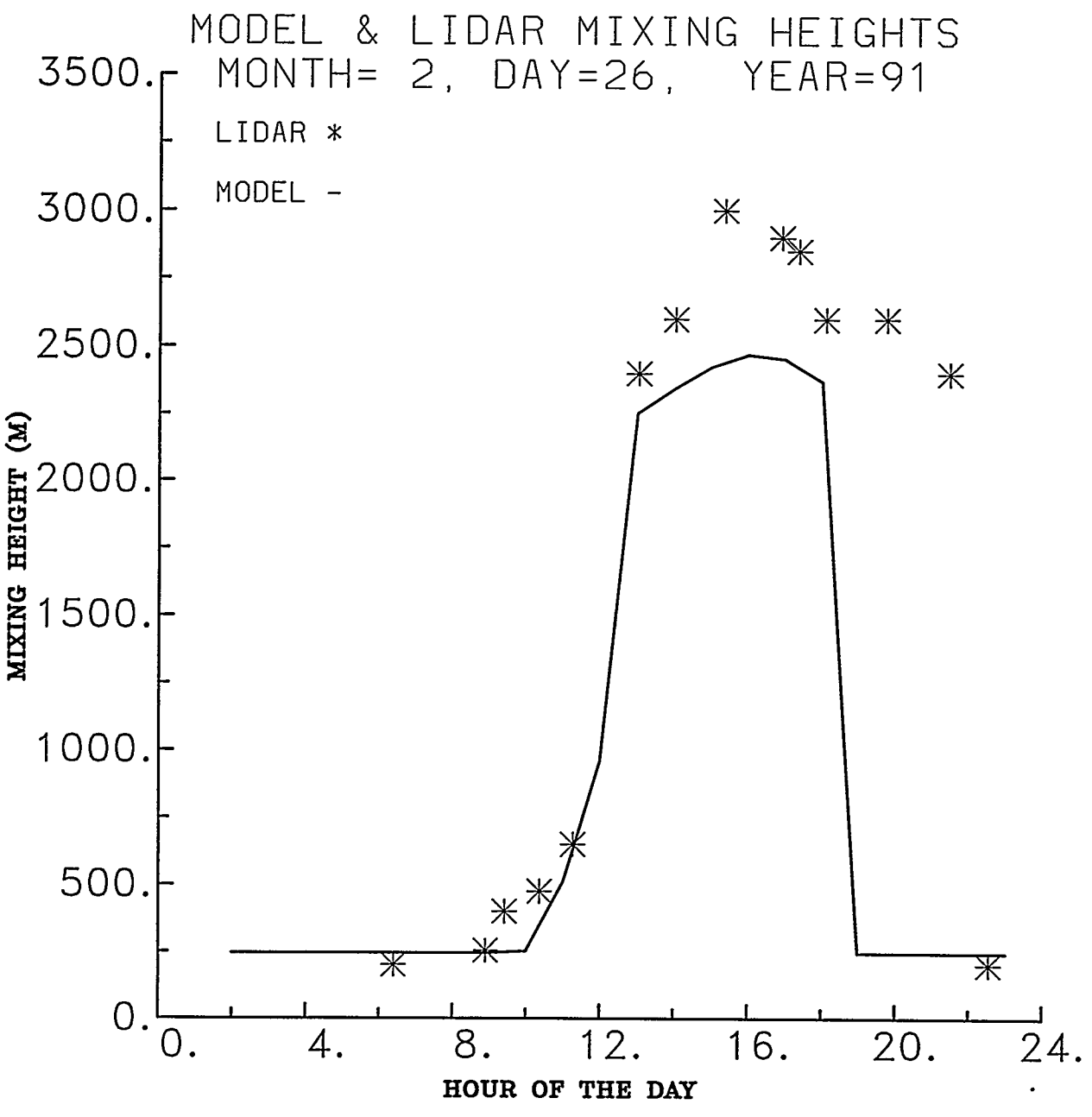
MODEL & LIDAR MIXING HEIGHTS
MONTH= 2, DAY=26, YEAR=91
LIDAR *
MODEL -
3500.
3000.
2500.
2000.
1500.
1000.
500.
0.
MIXING HEIGHT (M)
0.
4.
8.
12.
16.
20.
24.
HOUR OF THE DAY

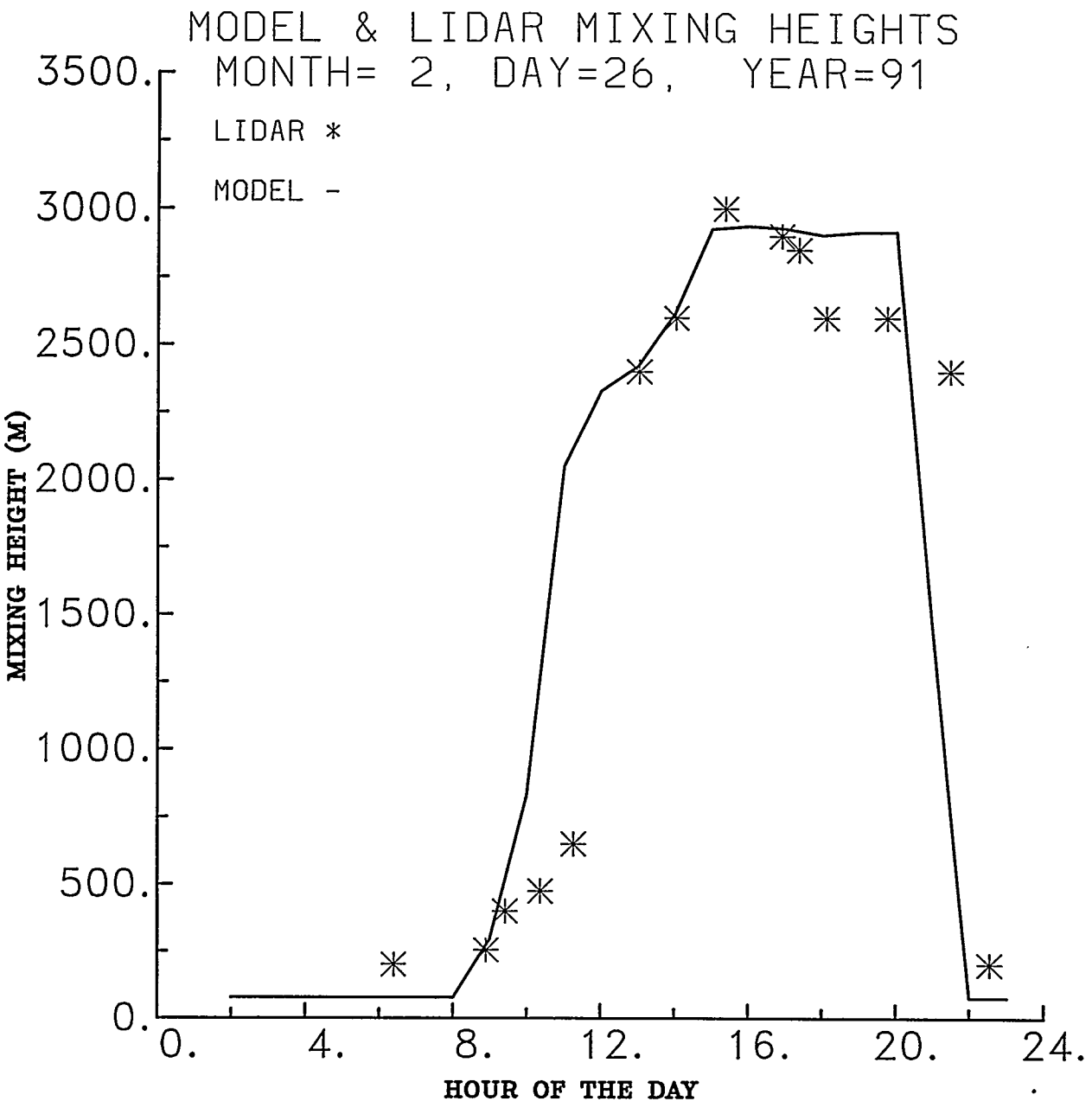
MODEL & LIDAR MIXING HEIGHTS
MONTH= 2, DAY=26, YEAR=91
LIDAR *
MODEL -
3500.
3000.
2500.
2000.
1500.
1000.
500.
0.
MIXING HEIGHT (M)
0.
4.
8.
12.
16.
20.
24.
HOUR OF THE DAY

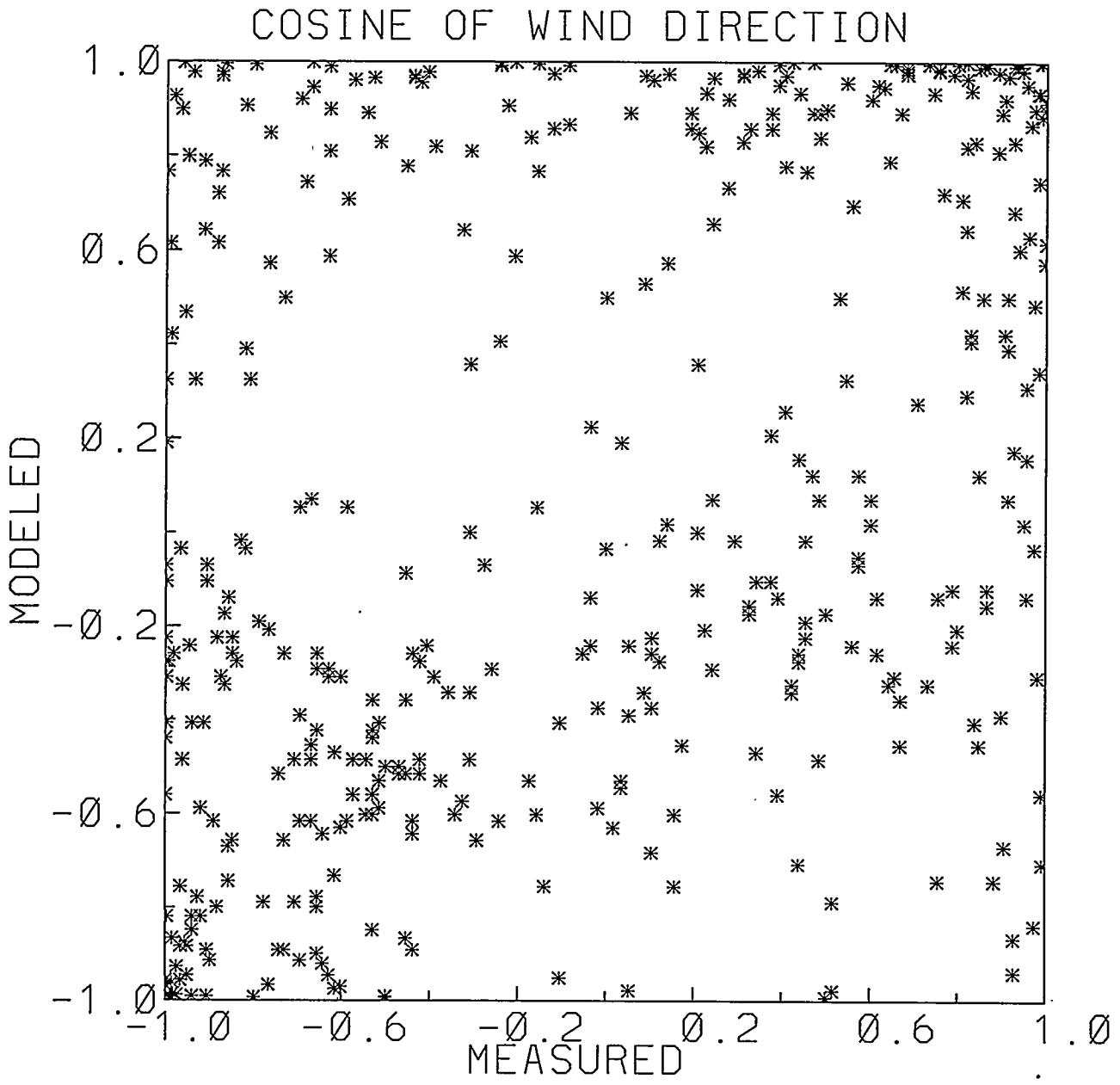
COSINE OF WIND DIRECTION
1.0
0.6
0.2
-0.2
-0.6
-1.0
MODELED
-1.0
-0.6
-0.2
0.2
0.6
1.0
MEASURED

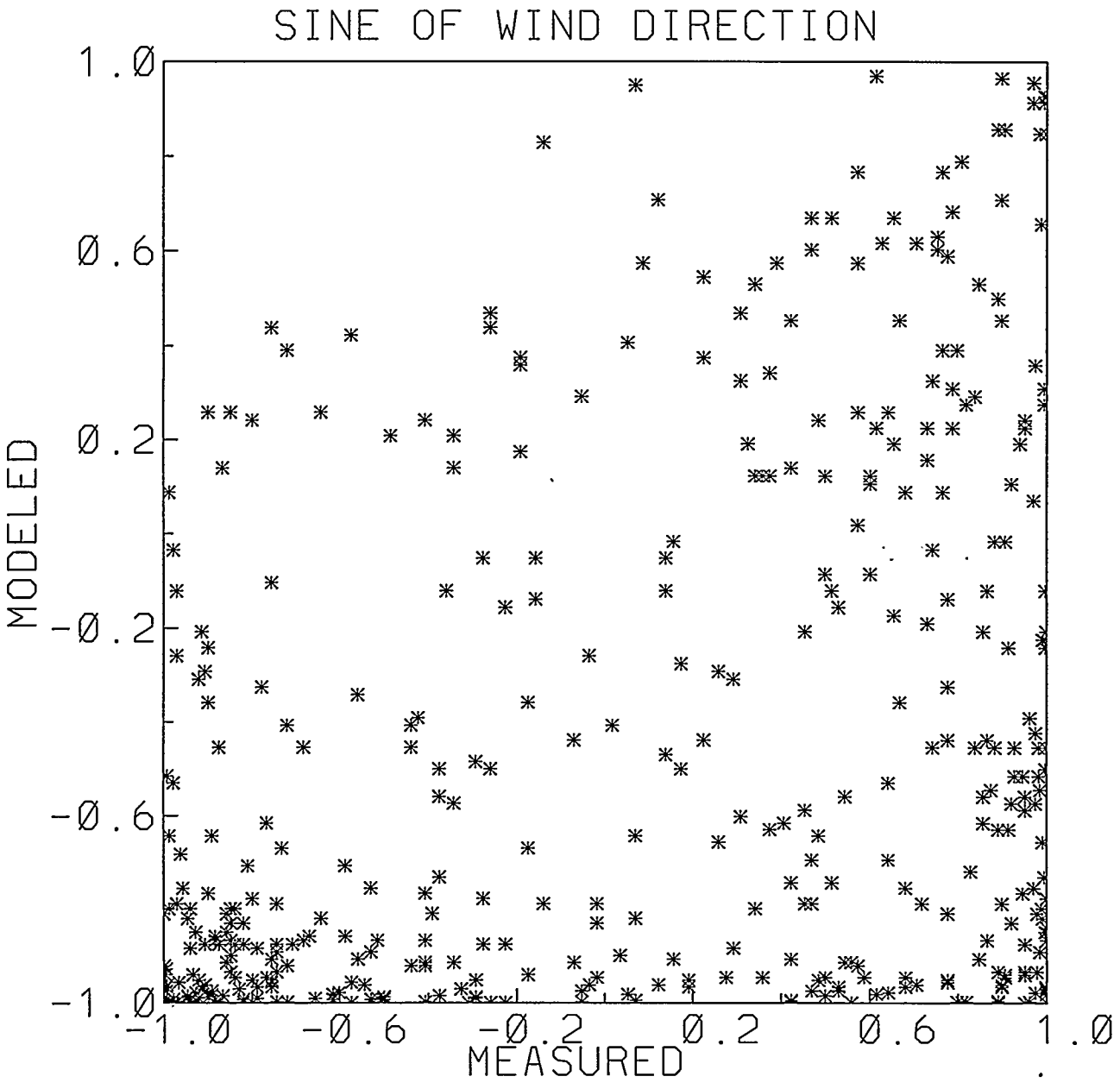
SINE OF WIND DIRECTION
1.0
0.6
0.2
-0.2
-0.6
-1.0
MODELED
-1.0
-0.6
-0.2
0.2
0.6
1.0
MEASURED

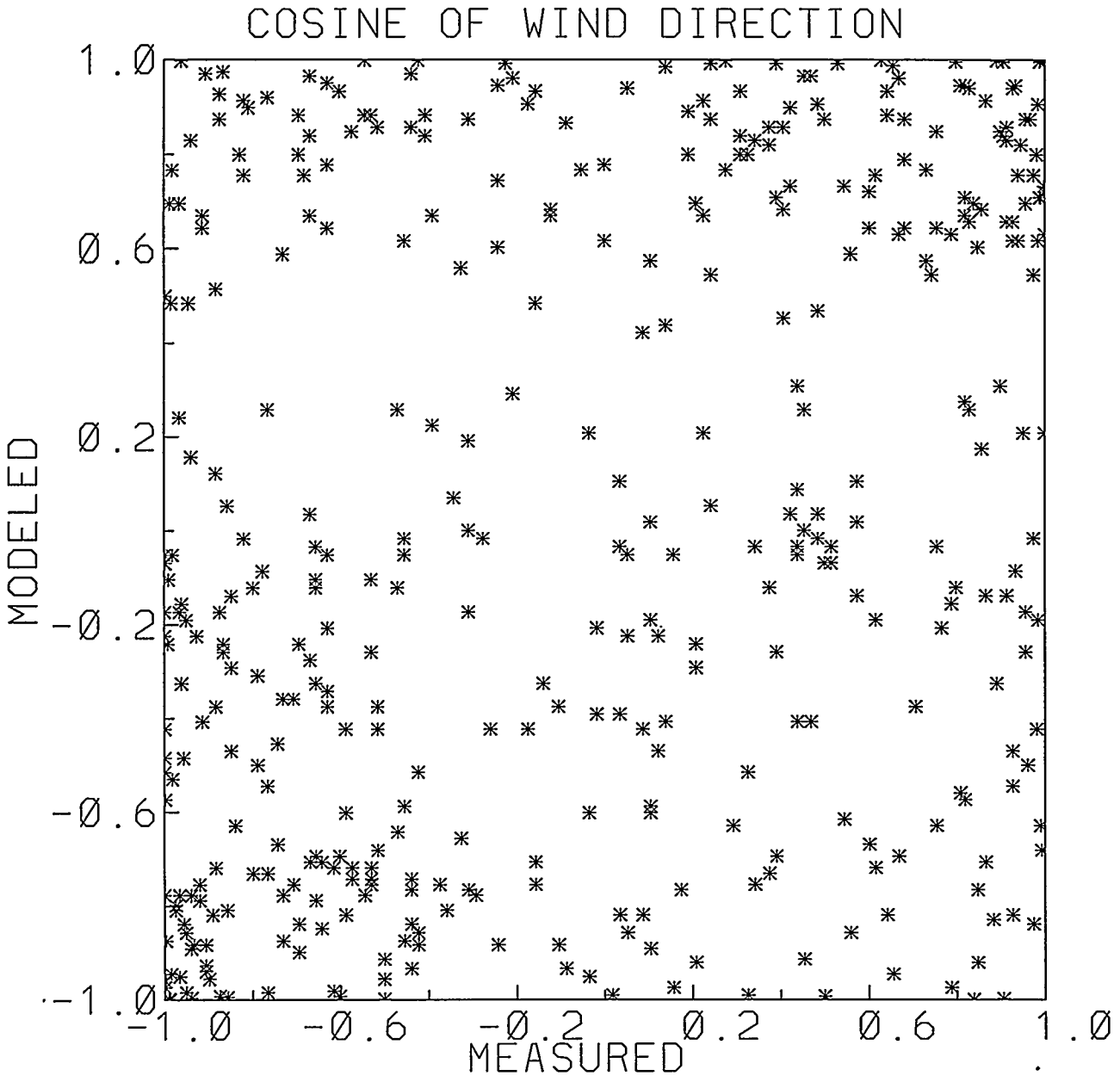
COSINE OF WIND DIRECTION
1.0
0.6
0.2
-0.2
-0.6
-1.0
MODELED
-1.0
-0.6
-0.2
0.2
0.6
1.0
MEASURED

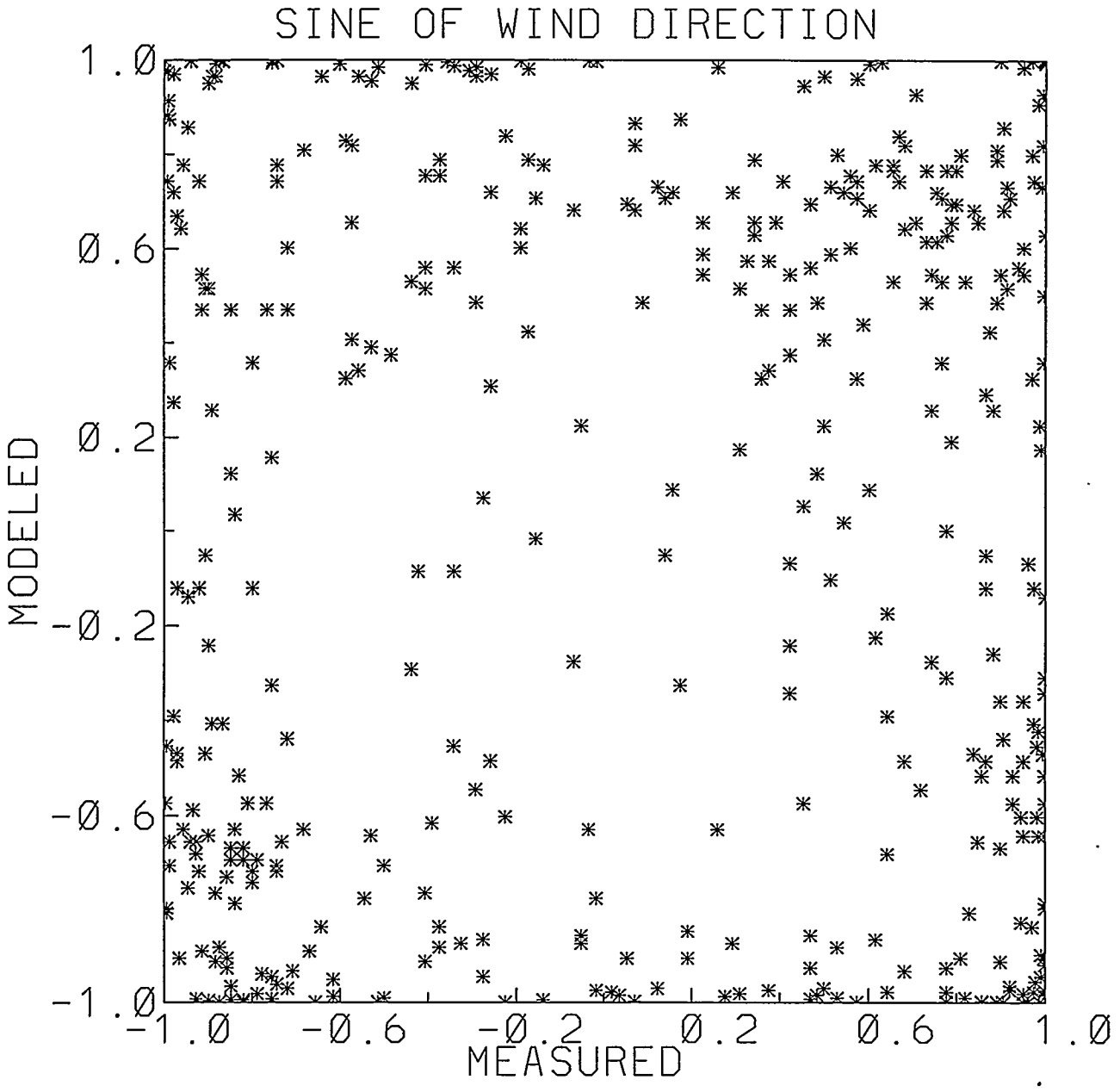
SINE OF WIND DIRECTION
1.0
0.6
0.2
-0.2
-0.6
-1.0
MODELED
-1.0
-0.6
-0.2
0.2
0.6
1.0
MEASURED

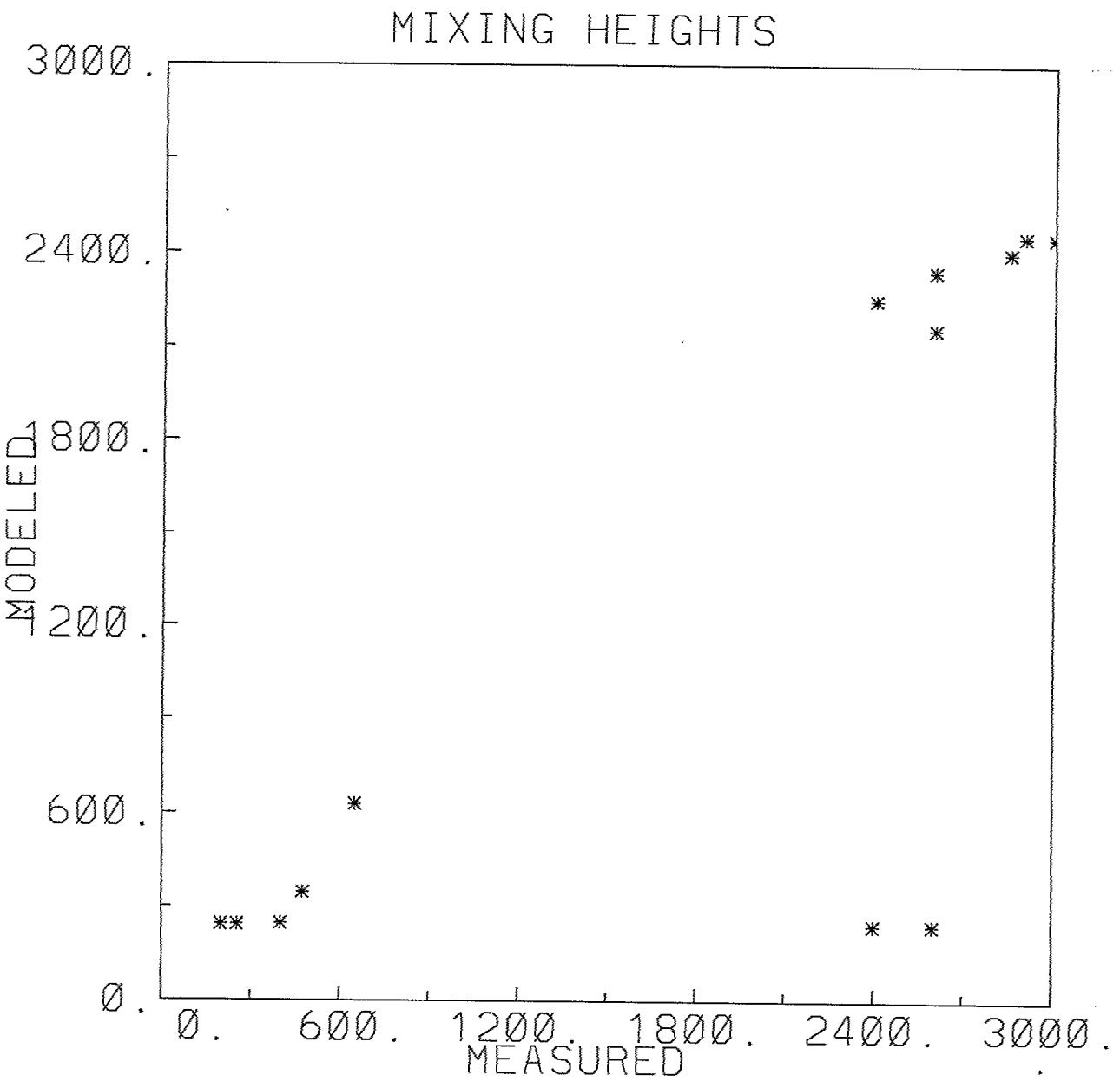
MIXING HEIGHTS
3000.
2400.
1800.
1200.
600.
0.
MODELED
0.
600.
1200.
1800.
2400.
3000.
MEASURED

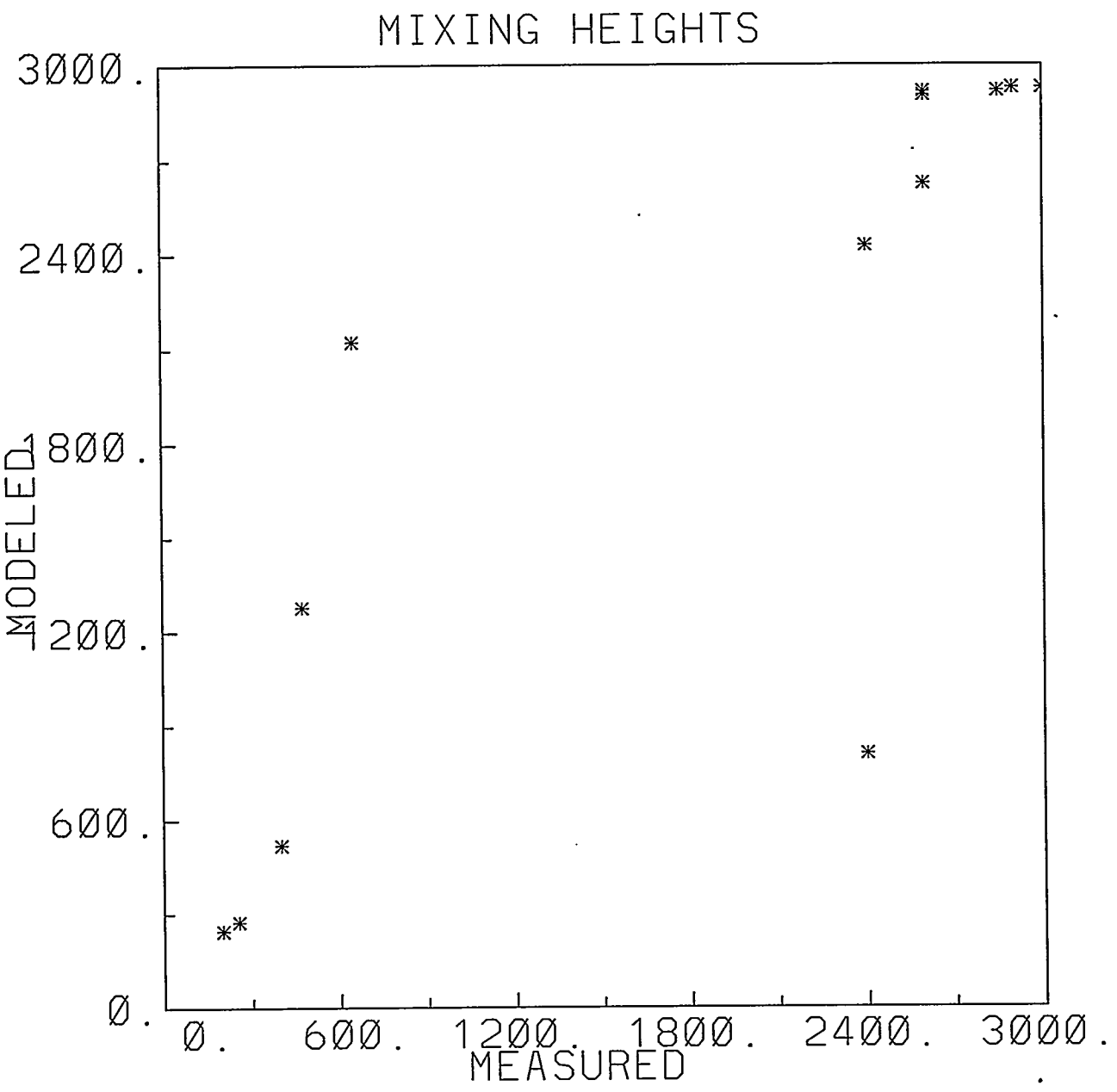
MIXING HEIGHTS
3000.
2400.
1800.
1200.
600.
0.
MODELED
0.
600.
1200.
1800.
2400.
3000.
MEASURED